

# Flows and mixing in channels with misaligned superhydrophobic walls

Tatiana V. Nizkaya,<sup>1,\*</sup> Evgeny S. Asmolov,<sup>1,2,\*</sup> Jiajia Zhou,<sup>3,\*</sup> Friederike Schmid,<sup>3</sup> and Olga I. Vinogradova<sup>1,4,5,†</sup>

<sup>1</sup>*A.N. Frumkin Institute of Physical Chemistry and Electrochemistry,*

*Russian Academy of Science, 31 Leninsky Prospect, 119991 Moscow, Russia*

<sup>2</sup>*Central Aero-Hydrodynamic Institute, 140180 Zhukovsky, Moscow region, Russia*

<sup>3</sup>*Institut für Physik, Johannes Gutenberg-Universität Mainz, D55099 Mainz, Germany*

<sup>4</sup>*Department of Physics, M.V. Lomonosov Moscow State University, 119991 Moscow, Russia*

<sup>5</sup>*DWI - Leibniz Institute for Interactive Materials,*

*RWTH Aachen, Forckenbeckstr. 50, 52056 Aachen, Germany*

(Dated: December 7, 2024)

Aligned superhydrophobic surfaces with the same texture orientation reduce drag in the channel and generate secondary flows transverse to the direction of the applied pressure gradient. Here we show that a transverse shear, superimposed with the conventional Poiseuille and slip-driven plug flows, can be easily generated by using superhydrophobic channels with misaligned textured surfaces. We propose a general theoretical approach to quantify this transverse flow by introducing the concept of an effective shear tensor. To illustrate its use, we present approximate theoretical solutions and Dissipative Particle Dynamics simulations for striped superhydrophobic channels. Our results demonstrate that the transverse shear leads to complex flow patterns on the length scale of the texture period, which leads to a new mechanism of a passive mixing at low Reynolds number. This vertical mixing occurs at the texture period scale and does not require the contribution of side walls. Our results provide a basis for design and analysis of mixing properties of superhydrophobic channels with arbitrary oriented textures.

PACS numbers: 83.50.Rp, 47.11.-j, 47.61.-k, 47.61.Ne

## I. INTRODUCTION

Superhydrophobic (SH) textures have raised a considerable interest and motivated numerous studies during the past decade [1, 2]. Such surfaces in the Cassie state, i.e., where the texture is filled with gas, are extremely important in the context of fluid dynamics due to their superlubricating potential [3–5]. The use of highly anisotropic SH textures provides additional possibilities for flow manipulation. The effective hydrodynamic slip of such surfaces,  $\mathbf{b}_{\text{eff}}$ , is generally tensorial [6–9] due to secondary flows transverse to the direction of the applied pressure gradient [10, 11]. This can be used to separate particles [12] and enhance mixing rate [13] in typical for microfluidic devices low-Reynolds-numbers flows. Over the last decade, the quantitative understanding of liquid flow in anisotropic SH channels was significantly expanded. However, many fundamental issues still remain challenging.

According to the modern concept of effective slip,  $\mathbf{b}_{\text{eff}}$  is a global characteristic of a channel [5], which can be applied for arbitrary channel thickness [9]. This implies that the eigenvalues depend not only on the parameters of the heterogeneous surfaces (such as local slip lengths, fractions of phases, and the texture period  $L$ ), but also on the channel thickness  $H$ . However, for a thick (compared to  $L$ ) channel they become a characteristics of a

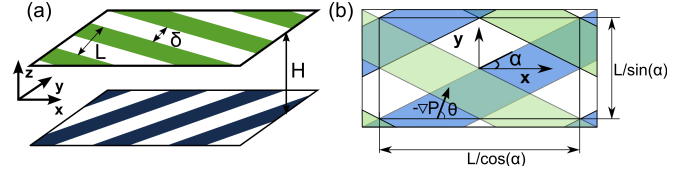


FIG. 1: (a) Cartoon showing the two identical misaligned superhydrophobic walls decorated with no-slip (white) and partial-slip (colored) stripes. (b) Top view of periodic rectangular unit cell.

heterogeneous interface solely [3, 7, 14].

Most of the prior work has focused on the optimization of the (forward) effective slip and calculations of the eigenvalues of the effective slip-length tensor for a single 1D interface [15–19] and channels with aligned walls [8, 20] or one hydrophilic (no-slip) wall [8, 9]. The eigenvalues of  $\mathbf{b}_{\text{eff}}$  correspond to the directions of fastest and lowest effective slip. In these directions, a pressure gradient does not produce transverse flows. In other directions, however, a flow may become misaligned with the force, and transverse hydrodynamic flow can be generated. This was discussed for a single interface [5, 7], for channels with symmetrically aligned stripes [10, 20] or with one no-slip wall [10, 21].

In the present paper, we address a different phenomenon, which has not been appreciated in previous work [7]: The possibility to generate *shear* flow with anisotropic SH textures. We consider channels with identical, but misaligned textured and anisotropic walls and show that any misalignment necessarily leads to a generation of shear flow in the transverse direction. This

\*These three authors contributed equally to the work.

†Corresponding author: oivinograd@yahoo.com

is derived with general theoretical arguments and confirmed by Dissipative Particle Dynamics (DPD) simulations. The transverse shear, in turn, generates complex flow structures at the scale of the texture period. Simulation results show that, at finite Reynolds numbers of the flow, these small-scale structures lead to global mixing of fluids from the lower and the upper parts of the channel. This mechanism of mixing does not rely on the presence of confining side walls, therefore its efficiency does not depend on the aspect ratio of the channel.

## II. THEORY

We consider the pressure-driven Stokes flow between two parallel stationary (passive) SH walls separated by the distance  $H$  and decorated with identical anisotropic textures of a period  $L$ , and assume the interface to be flat with no meniscus curvature (see Fig. 1(a)). Such an idealized situation, which neglects an additional mechanism for a dissipation due to a meniscus, has been considered in most previous publications [11, 18, 22] and observed in recent experiments [23]. We then impose no-slip at the solid area, i.e. neglect slippage of liquid [24–26] and gas [27] past hydrophobic surface, which is justified provided the nanometric slip is small compared to parameters of the texture. Prior work often assumed idealized shear-free boundary conditions over the gas sectors [22, 28, 29], so that the viscous dissipation in the underlying gas phase has been neglected. Here we will use the partial slip boundary conditions, which are the consequences of the ‘gas cushion model’ [30]. The lower and the upper wall textures are misaligned by an angle  $2\alpha$ . The flow is periodic with a rectangular unit cell as depicted in Fig. 1(b). We place the origin of the  $(x, y, z)$  coordinate system at the center of the cell, in the mid-plane, with the  $z$  axis perpendicular to the walls.

To address effective (‘macroscopic’) properties of the channel we evaluate the mean velocity profile, averaged over the periodic cell in  $x, y$ . Due to the linearity of the Stokes equations, it is sufficient to consider only the flow in eigendirections of the texture. Let us first consider a flow under a pressure gradient,  $\nabla P$ , aligned with the  $x$  axis ( $\theta = 0$ ). The flow in the transverse direction can be then obtained by replacing  $\alpha$  by  $\pi/2 - \alpha$ . The symmetry of the problem implies that the  $x$ -component of the average velocity is symmetric in  $z$  and its  $y$ -component is skew-symmetric. For the Stokes flow the mean velocity profile is scaled by  $U_0 = -H^2 \nabla P / (2\mu)$  and has the following form:

$$\langle \mathbf{u} \rangle(z) = \left( \frac{1}{4} - z^2 \right) \mathbf{e}_x + u_{sx} \mathbf{e}_x + \gamma_{yx} z \mathbf{e}_y. \quad (1)$$

Here the coordinates are scaled by  $H$ , the first term corresponds to an undisturbed Poiseuille flow, the second term is a plug flow in the direction parallel to the pressure gradient, and the last term represents a linear shear

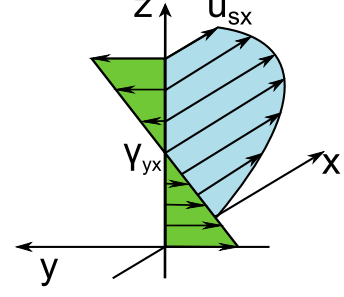


FIG. 2: Averaged velocity profile  $\langle \mathbf{u} \rangle(z)$  for the pressure gradient directed along  $-x$ , see Eq. (1).

flow in the transverse direction. Thus, the laminar flow in the channel in response to an applied pressure gradient is a linear superposition of these three terms as illustrated in Fig. 2. Eq.(1) can therefore be seen as a generalization of an earlier idea, formulated for a thick channel [7], to an arbitrary channel situation.

To quantify the effective properties of the channel, we now introduce the flow and shear rates averaged over the cell volume  $V$ :

$$\mathbf{Q} = \frac{1}{V} \int \mathbf{u}_\tau dV = -\frac{H^2}{12\mu} \mathbf{k} \cdot \nabla P, \quad (2)$$

$$\mathbf{G} = \frac{1}{V} \int \frac{\partial \mathbf{u}_\tau}{\partial z} dV = -\frac{H}{2\mu} \boldsymbol{\gamma} \cdot \nabla P, \quad (3)$$

where  $\mathbf{u}_\tau = (u_x, u_y)$  is the tangential velocity. The dimensionless permeability  $\mathbf{k}$  and shear  $\boldsymbol{\gamma}$  tensors can then be found by solving a local problem in the channel.

Let us note that Eq. (1) and the symmetry conditions imply that the tensors  $\mathbf{k}$  and  $\boldsymbol{\gamma}$  are:

$$\mathbf{k} = \begin{pmatrix} k_{xx}(\alpha) & 0 \\ 0 & k_{yy}(\alpha) \end{pmatrix}, \quad (4)$$

where  $k_{xx} = 1 + 6u_{sx}$  and

$$\boldsymbol{\gamma} = \begin{pmatrix} 0 & \gamma_{xy}(\alpha) \\ \gamma_{yx}(\alpha) & 0 \end{pmatrix}. \quad (5)$$

Thus, our choice of coordinate system diagonalizes the permeability tensor. Also, due to the symmetry of the periodic cell,  $k_{yy}(\alpha) = k_{xx}(\pi/2 - \alpha)$  and  $\gamma_{xy}(\alpha) = \gamma_{yx}(\pi/2 - \alpha)$ .

To calculate  $u_{sx}(\alpha)$  and  $\gamma_{yx}(\alpha)$  we have to solve the Stokes equations on the periodic cell with spatially varying local slip lengths modelling the SH textures. We assume that the gap of the channel is large enough, so that the perturbation of the flow due to texture of one wall is small at the opposite wall. In this case, the hydrodynamic interaction between the two walls is mainly mediated by the mean flow, and the periodic perturbation can be considered as a sum of two solutions for a configuration with one SH and one hydrophilic wall. This simplification allows us to obtain explicit formulae for

the average slip and the shear tensor (the details of the calculation are given in the Appendix A):

$$u_{sx}(\alpha) = \frac{\beta_+ + \beta_- \cos(2\alpha) + 2(\beta_+^2 - \beta_-^2)}{1 + 2\beta_+ - 2\beta_- \cos(2\alpha)}, \quad (6)$$

$$\gamma_{yx}(\alpha) = -\frac{2\beta_- \sin(2\alpha)}{1 + 2\beta_+ - 2\beta_- \cos(2\alpha)}, \quad (7)$$

where  $\beta_+ = (b_{\text{eff}}^{\parallel} + b_{\text{eff}}^{\perp})/(2H)$ ,  $\beta_- = (b_{\text{eff}}^{\parallel} - b_{\text{eff}}^{\perp})/(2H)$ . The effective slip tensor  $\mathbf{b}_{\text{eff}}$  here corresponds to a configuration with one SH wall.

The misalignment of the top and the bottom textures leads to a ‘macroscopic’ anisotropy of the flow: The channel permeability depends on the direction of the pressure gradient, and a secondary flow in transverse direction is generated. To study this effect, we consider flow under a pressure gradient  $\nabla P$  imposed at an angle  $-\theta$  to the  $x$ -axis (the driving force of the flow is in the opposite direction).

For the fluxes in the direction opposite to the pressure gradient and in the transverse direction we obtain, using the tensorial formalism [7]:

$$\begin{aligned} Q_L/Q_0 &= k_{xx} \cos^2 \theta + k_{yy} \sin^2 \theta, \\ Q_T/Q_0 &= (k_{xx} - k_{yy}) \cos \theta \sin \theta, \end{aligned} \quad (8)$$

where  $Q_0 = \frac{|\nabla P|H^2}{12\mu}$  corresponds to the Poiseuille flow through a channel with hydrophilic walls.

Similarly, for the mean shear rates we get

$$\begin{aligned} G_L/G_0 &= -(\gamma_{xy} + \gamma_{yx}) \sin \theta \cos \theta, \\ G_T/G_0 &= \gamma_{yx} \cos^2 \theta - \gamma_{xy} \sin^2 \theta, \end{aligned} \quad (9)$$

where  $G_0 = \frac{U_0}{H} = \frac{|\nabla P|H}{2\mu}$  is a characteristic shear rate for a hydrophilic channel. From Eq. (9), it follows that the transverse shear rate  $G_T$  becomes zero for two angles  $\theta = \pm(\arctan(\gamma_{xy}/\gamma_{yx}))^{1/2}$ . However, this does not imply that the shear tensor can be diagonalized by a proper rotation of the coordinate system, since the two directions are not orthogonal in the general case.

To illustrate this general approach we focus below on specific case of 1D SH surfaces consisting of periodic stripes, where the piecewise constant local slip lengths of (identical) textured walls vary in only one direction.

### III. SIMULATION METHOD

We apply the Dissipative Particle Dynamics (DPD) method [31, 32] to simulate the flow inside a channel with striped SH walls. DPD is an established coarse-grained, momentum-conserving, mesoscopic method for fluid simulation. Since it is also a particle-based method, thermal fluctuations are naturally included. More specifically, we use DPD as a thermostat without conservative interactions [33], and combine that with a tunable-slip method [34] that allows one to vary the local slip

length [16, 20, 35]. In the following, physical quantities will be reported in a model unit system of  $\sigma$  (length),  $m$  (mass), and  $\varepsilon = k_B T$  (energy).

For misaligned striped surfaces, it is important to note that the simulation box depends on the misalignment angle  $2\alpha$  due to the periodic boundary conditions in the directions parallel to the patterned surfaces ( $x$  and  $y$  in Fig. 1). The three dimensions of the simulation box are  $(L/\sin \alpha, L/\cos \alpha, H + 2\sigma)$ , where the extra  $2\sigma$  in  $z$ -direction accounts for the depletion due to the excluded volume interaction of the impermeable surfaces. In the present study, we have used a stripe spacing  $L = 20\sigma$  and channel widths  $H = L$  and  $H = L/2$ . With a fluid density  $\rho = 3.75\sigma^{-3}$ , a typical system consists of  $0.6\text{--}1.2 \times 10^5$  particles. The simulation starts with randomly distributed particles. The pressure-driven flow is modeled by applying an external force to all particles. The system is allowed to reach a steady state after  $10^6$  time steps; then the measurement is performed by averaging over  $10^5$  time steps to obtain sufficient statistics. We use a small body force  $(0.001\varepsilon/\sigma$  for  $H = L$  and  $0.004\varepsilon/\sigma$  for  $H = L/2$ ) to ensure that the flow velocity is smaller than  $0.5\sqrt{\varepsilon/m}$ . The typical Reynolds number is  $\text{Re} \approx 2.8$ .

The simulations were carried out using the open source simulation package ESPResSo [36]. All simulations were performed with a time step  $\Delta t = 0.01\sqrt{m/\varepsilon}\sigma$ , and the temperature of the system was set at  $k_B T = 1\varepsilon$ . The DPD interaction parameter is chosen at  $\gamma_{\text{DPD}} = 5.0\sqrt{m\varepsilon}/\sigma$  and the cutoff is  $1.0\sigma$ . The shear viscosity is measured to be  $\mu_s = 1.35 \pm 0.01\sqrt{m\varepsilon}/\sigma^2$ .

### IV. RESULTS AND DISCUSSION

In order to assess the validity of the above theoretical approach we run a set of simulations in channels with different misalignment angles  $\alpha$  and two gaps  $H/L = 1$  and  $H/L = 0.5$ . All simulations have been performed for textures with the fraction of gas phase  $\phi = \delta/L = 1/2$  and a local slip length  $b/L = 10$ . By averaging the simulation data over the periodic cell, we calculate the mean fluxes and shear rates for different directions of the pressure gradient  $\theta$  and several misalignment angles  $\alpha$ . The simulation results are shown in Fig. 3. Also included are the fluxes and shear rates calculated using Eqs. (8-9). In this case the tensors  $\mathbf{k}$  and  $\boldsymbol{\gamma}$  have been found using the numerical solutions of the Stokes equations [21] (see Appendix A for details). A general conclusion is that the theoretical predictions are in excellent agreement with simulation results for  $H = L$  (Fig. 3(a,b)). Even for thinner channels,  $H = L/2$  (Fig. 3(c,d)), where the theory slightly underestimates the permeability and overestimates the transverse shear, the agreement is quite good. This is probably due to the fact that the interactions between pattern-induced flow perturbations on opposing walls have been neglected, as explained in Section II. These interactions become more important as

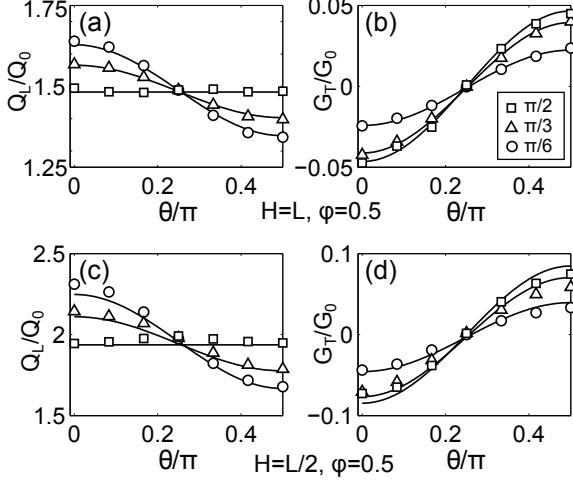


FIG. 3: Flow rate in the direction of pressure gradient (a, c) and shear rate in the transverse direction (b, d) computed with  $b/L = 10$  as a function of angle  $\theta$ . The upper graphs (a, b) correspond to a channel with  $H = L$ , and the lower graphs (c, d) to  $H = L/2$ . Solid curves are the theoretical predictions (Eqs. (8) and (9)), and symbols are the simulation results for misalignment angles  $2\alpha = \pi/6$  (circles),  $\pi/3$  (triangles), and  $\pi/2$  (squares).

$H$  decreases. The flow rates  $Q_L$  become maximal and minimal for pressure gradients pointing along the  $x$  and  $y$  axis, respectively. These directions are also those of largest transverse shear  $G_T$ . When the stripes on the lower and the upper walls are orthogonal ( $\alpha = \pi/4$ ) we have  $k_{xx} = k_{yy}$ , and  $Q_L$  does not depend on the direction of pressure gradient, while  $Q_T = 0$ . However, this does not imply that no transverse flow is generated in this configuration. Indeed, the transverse shear rate  $G_T$  is actually maximal in this case.

The texture misalignment leads to a complex flow on the scale of the period of the texture. To analyze the flow structure we consider in detail the case  $\alpha = \pi/4$ ,  $\theta = 0$  for  $H = L/2$ . In this case the transverse flux is zero, but the transverse shear is maximal. Fig. 4 shows a projection of local velocity field onto the  $yz$ -plane at three sections of the periodic cell,  $x = 0$ ,  $x = L_x/8$  and  $x = L_x/4$ , calculated from the simulation data. Guided by the texture, the fluid is driven to the right (in the direction of positive  $y$ ) in the upper part of the channel and to the left in the lower part. The velocity field has a significant vertical component which enables fluid particles to move between the upper and the lower parts of the channel. We also observe two saddle points with strain-like flows around each of them. In 2D flows such structures are potentially good for stirring, because close fluid trajectories diverge in the vicinity of saddle points. Note however that in a 3D flow global behavior of fluid trajectories can not be predicted from local snapshots of the velocity field.

To understand the global properties of this flow, we

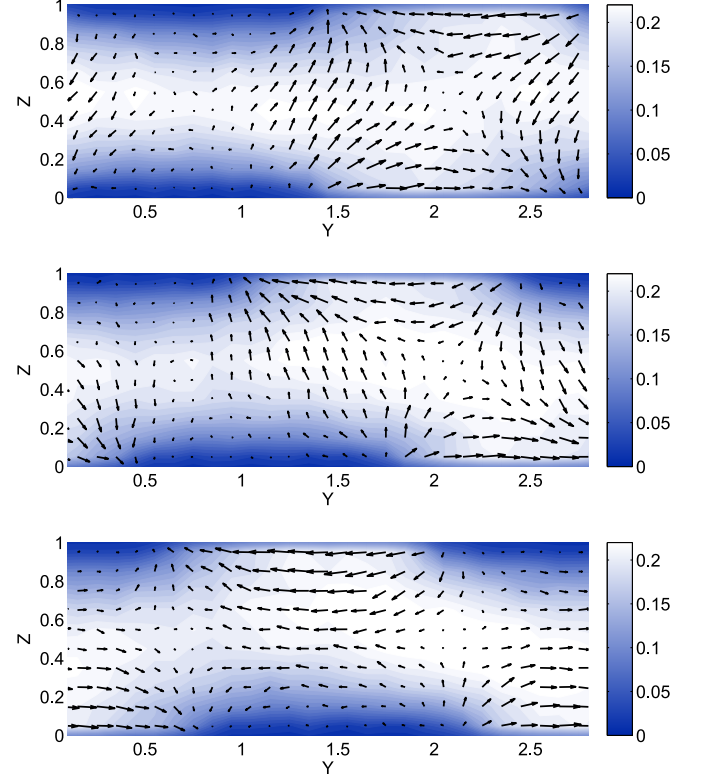


FIG. 4: Front view of the simulated velocity field ( $u_y, u_z$ ) in the cross-sections  $x = 0$ ,  $\sqrt{2}L/8$ , and  $\sqrt{2}L/4$  (from top to bottom). Color map shows the longitudinal velocity  $u_x$ .

calculate the flow streamlines by releasing fluid particles at  $x = 0$  and tracking their positions down to the end of the periodic cell,  $x = L_x$ . Some of these streamlines are depicted in Fig. 5. Even though fluid particles follow the periodic velocity field, they reach different positions on the  $yz$ -plane after crossing one unit cell, see Fig. 5(c). Two general features are observed. First, the fluid particles are displaced in the  $y$  direction. This reflects the non-zero average shear in the system. Second, one also observes a small (but non-zero) vertical displacement. This vertical displacement is crucial for the mixing properties of the channel. Every point at the beginning of the period  $\mathbf{r}_0 = (0, y_0, z_0)$  is mapped to some point at the end of the period  $\mathbf{r}_1 = (L_x, y_1, z_1)$ . Since the flow is periodic, the positions of fluid particles over many periods can be predicted by applying this mapping repeatedly. The displacement of a fluid particle is defined only by its initial position and can be defined as a vector field:  $\Delta r_k^{y,z} = J_{y,z}(y_k, z_k)$ . It is this displacement field (rather than the local velocity field), that characterizes the flow and its potential mixing properties.

Figure 6(a) shows the displacement field computed for the theoretical velocity field at  $\text{Re} \ll 1$  ( $\mathbf{u}$  is obtained by the numerical solution of the Stokes equations, see Appendix A). The vertical displacement is small in this case. The field  $J_{y,z}(y, z)$  for simulated streamlines at  $\text{Re} = 2.8$  is plotted in Fig. 6(b). The vector field at finite



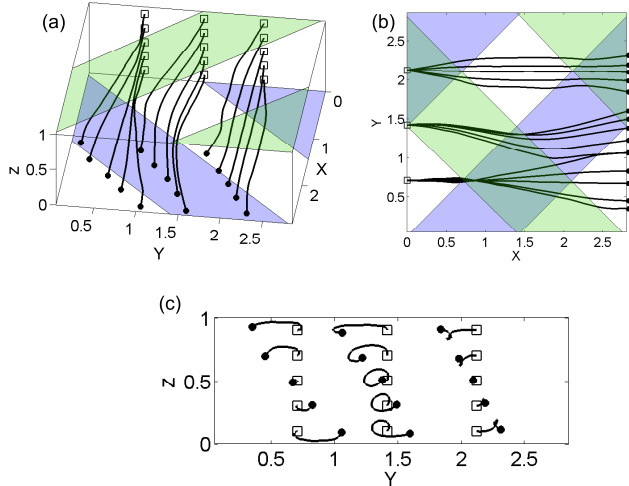


FIG. 5: Streamlines for the simulated velocity field: 3D view (a), top view (b) and front view (c). Squares indicate initial positions of fluid particles and dots their positions at the end of the periodic cell.

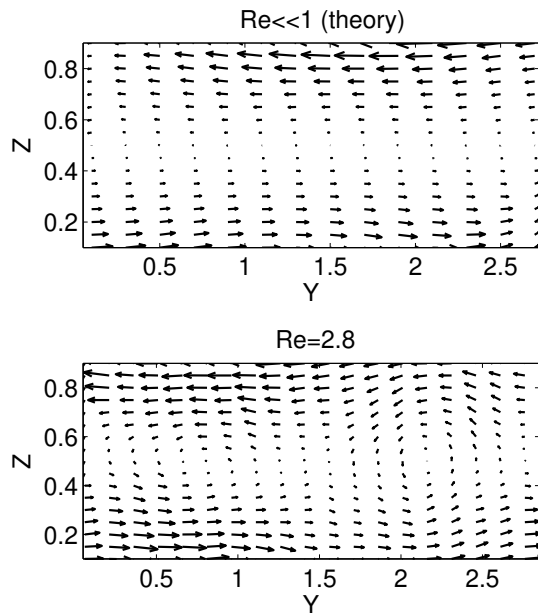


FIG. 6: Displacement of fluid particles over one cell period in  $yz$ -plane. The velocity fields are obtained from simplified theory for  $Re \ll 1$  and simulations for  $Re = 2.8$ .

fluid inertia has a structure of two co-rotating vortices combined with a uniform shear. Such a flow can stir the fluid between the upper and the lower part in the central zone of the channel, while in near-wall zones the fluid is transported in the transverse direction. In this particular case the rotational component is relatively small, but we expect it to grow, with increasing Reynolds number in

the channel.

We recall that our calculations were done for channels infinitely extended in the  $y$  direction. In the presence of confining side walls, the shear flow will of course additionally induce vertical recirculation currents along these walls. However, far from the walls the flow will remain the same since no pressure gradient is generated in transverse direction.

## V. CONCLUSION

In this paper we have extended the tensorial description of SH channels developed earlier to configurations with misaligned textures on bottom and top walls. The effective properties of such channels are described by two tensors: the permeability tensor  $\mathbf{k}$  and the shear rate tensor  $\gamma$ . These tensors have been calculated using two complementary approaches: The simplified analytical model, in which periodic perturbations of the velocity field due to opposing textured walls are assumed to be independent, and DPD simulations. The theoretical approach has provided good accuracy for channel thickness down to a half of the texture period.

Simulations have shown that at finite Reynolds number the flow generated by this transverse shear can mix the fluids in upper and lower parts of the channel. This effect is expected to become stronger for increasing Reynolds number. The analysis of the different regimes will be a subject of a separate study. Unlike most classical mixers with one patterned wall [4, 37], where the roll structures are created by the side walls of the channel, in our misaligned configuration the mixing occurs on the scale of the texture period. This provides a basis for a new mixing mechanism which does not depend on the presence of confining side walls and is therefore insensitive to the cross-sectional aspect ratio of the channel.

Finally, we mention that our results can be immediately extended to a situation of a channel with a periodically changing orientation of top and bottom stripes, which could lead to a chaotic advection [38–40], currently exploited mostly in the ‘herringbone’-type mixers [37].

## Acknowledgments

This research was partly supported by the RAS through its priority program ‘Assembly and Investigation of Macromolecular Structures of New Generations’, and by the VW foundation. The simulations were carried out using computational resources at the John von Neumann Institute for Computing (NIC Jülich), the High Performance Computing Center Stuttgart (HLRS) and Mainz University (MOGON).

### Appendix A: Calculation of tensors $\mathbf{k}$ and $\gamma$ for finite channel width

We write the velocity field in the cell  $\mathbf{u}(x, y, z) = (u_x, u_y, u_z)$  in the form

$$\mathbf{u} = \langle \mathbf{u} \rangle + \mathbf{u}_1 + \mathbf{u}_2. \quad (\text{A1})$$

Here  $\mathbf{u}_1$ ,  $\mathbf{u}_2$  are perturbations with zero mean over the cell volume generated by the non-homogeneous slippage on the bottom and top walls, respectively.

Because of the linearity of the problem the boundary conditions for  $\mathbf{u}_1$ ,  $\mathbf{u}_2$  at the bottom wall can be set as

$$\begin{aligned} z = -\frac{1}{2} : \quad & \mathbf{u}_2 = \mathbf{0}, \quad u_{z1} = 0, \\ & \mathbf{u}_{\tau 1} - b_1 \frac{\partial \mathbf{u}_{\tau 1}}{\partial z} = -u_{sx} \mathbf{e}_x + \frac{\gamma_{yx}}{2} \mathbf{e}_y \\ & + b_1 \left( \mathbf{e}_x + \gamma_{yx} \mathbf{e}_y + \frac{\partial \mathbf{u}_{\tau 2}}{\partial z} \right), \end{aligned} \quad (\text{A2})$$

and at the top wall as

$$\begin{aligned} z = \frac{1}{2} : \quad & \mathbf{u}_1 = \mathbf{0}, \quad u_{z2} = 0, \\ & \mathbf{u}_{\tau 2} - b_2 \frac{\partial \mathbf{u}_{\tau 2}}{\partial z} = -u_{sx} \mathbf{e}_x - \frac{\gamma_{yx}}{2} \mathbf{e}_y \\ & + b_2 \left( -\mathbf{e}_x + \gamma_{yx} \mathbf{e}_y + \frac{\partial \mathbf{u}_{\tau 1}}{\partial z} \right), \end{aligned} \quad (\text{A3})$$

where  $b_{1,2}(x, y)$  are the local slip lengths on the lower and the upper wall, respectively.

The perturbations decay at a distance from the wall of the order  $L$ . For this reason we can expect, for a sufficiently thick channel, that the disturbance gradients at the opposite walls are small:

$$\begin{aligned} z = -\frac{1}{2} : \quad & \left| \frac{\partial \mathbf{u}_{\tau 1}}{\partial z} \right| \ll \left| \frac{\partial \langle \mathbf{u} \rangle}{\partial z} \right|, \\ z = \frac{1}{2} : \quad & \left| \frac{\partial \mathbf{u}_{\tau 2}}{\partial z} \right| \ll \left| \frac{\partial \langle \mathbf{u} \rangle}{\partial z} \right|. \end{aligned} \quad (\text{A4})$$

In other words, we take into account the interaction of SH walls mediated by the mean flow, but we neglect the contribution of the inhomogeneous part of the flow which decays with the distance from the wall. Then the solution is the superposition of two flows in a channel with a SH and a no-slip walls. These 2D flows can be calculated using the numerical solutions of Stokes equations [21]. The validity of the assumption, Eq.(A4), is verified by evaluating the disturbance gradients induced by a SH wall on a no-slip wall. The gradients are small compared to the wall gradient for the Poiseuille flow,  $|\partial \langle \mathbf{u} \rangle / \partial z| = 2$ , at  $H/L > 0.5$  (see Fig. 7).

Consider the flow induced by the undisturbed shear rate  $\mathbf{e}_x + \gamma_{yx} \mathbf{e}_y$  at the bottom wall. Projections of the unit vectors to the  $(\xi, \eta)$  coordinate system with the axes parallel and perpendicular to the stripes (see Fig. 8) are

$$\begin{aligned} \mathbf{e}_x &= \mathbf{e}_\xi \cos \alpha - \mathbf{e}_\eta \sin \alpha, \\ \mathbf{e}_y &= \mathbf{e}_\xi \sin \alpha + \mathbf{e}_\eta \cos \alpha. \end{aligned} \quad (\text{A5})$$

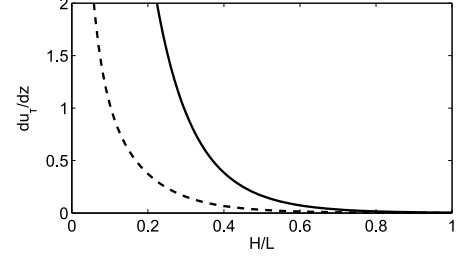


FIG. 7: Maximal values of the velocity disturbance gradient at the opposite wall for  $b/L = 10$ ,  $\phi = \delta/L = 1/2$ ,  $\alpha = \pi/4$  as a function of the channel width. Solid line is  $\frac{\partial u_{y1}}{\partial z}$ , dashed line is  $\frac{\partial u_{x1}}{\partial z}$  at  $z = 1/2$ .

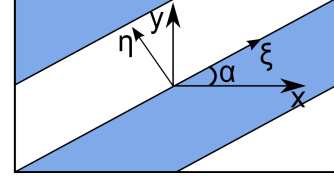


FIG. 8: Coordinate system  $(\xi, \eta)$ , associated with bottom wall stripes, see Eq.(A5).

In view of Eqs. (A3) and (A5), the mean slip velocity and the shear rate at  $z = -\frac{1}{2}$  are

$$\begin{aligned} \langle \mathbf{u}_\tau \rangle &= \left( u_{sx} \cos \alpha - \frac{\gamma_{yx}}{2} \sin \alpha \right) \mathbf{e}_\xi \\ &\quad - \left( u_{sx} \sin \alpha + \frac{\gamma_{yx}}{2} \cos \alpha \right) \mathbf{e}_\eta, \end{aligned} \quad (\text{A6})$$

$$\left\langle \frac{\partial \mathbf{u}_\tau}{\partial z} \right\rangle = (\cos \alpha + \gamma_{yx} \sin \alpha) \mathbf{e}_\xi - (\sin \alpha - \gamma_{yx} \cos \alpha) \mathbf{e}_\eta.$$

From (A6) we have

$$\frac{b_{\text{eff}}^{\parallel}}{H} = \frac{u_{sx} \cos \alpha - \frac{\gamma_{yx}}{2} \sin \alpha}{\cos \alpha + \gamma_{yx} \sin \alpha}, \quad (\text{A7})$$

$$\frac{b_{\text{eff}}^{\perp}}{H} = \frac{u_{sx} \sin \alpha + \frac{\gamma_{yx}}{2} \cos \alpha}{\sin \alpha - \gamma_{yx} \cos \alpha}. \quad (\text{A8})$$

Here the components of the effective slip length tensor  $\mathbf{b}_{\text{eff}}$  correspond to the usual configuration with a SH and a no-slip walls. Thus we obtain from (A7), (A8):

$$u_{sx}(\alpha) = \frac{\beta_+ + \beta_- \cos(2\alpha) + 2(\beta_+^2 - \beta_-^2)}{1 + 2\beta_+ - 2\beta_- \cos(2\alpha)}, \quad (\text{A9})$$

$$\gamma_{yx}(\alpha) = -\frac{2\beta_- \sin(2\alpha)}{1 + 2\beta_+ - 2\beta_- \cos(2\alpha)}, \quad (\text{A10})$$

where  $\beta_+ = (b_{\text{eff}}^{\parallel} + b_{\text{eff}}^{\perp})/(2H)$ ,  $\beta_- = (b_{\text{eff}}^{\parallel} - b_{\text{eff}}^{\perp})/(2H)$ .

The flow in the transverse direction can be obtained by replacing  $x$  by  $y$  and  $\alpha$  by  $\pi/2 - \alpha$ . Therefore, we readily obtain the permeability tensor:

$$\mathbf{k} = \begin{pmatrix} 1 + 6u_{sx}(\alpha) & 0 \\ 0 & 1 + 6u_{sx}(\pi/2 - \alpha) \end{pmatrix}, \quad (\text{A11})$$

and the shear tensor:

$$\gamma = \begin{pmatrix} 0 & \gamma_{yx}(\pi/2 - \alpha) \\ \gamma_{yx}(\alpha) & 0 \end{pmatrix}. \quad (\text{A12})$$

- 
- [1] D. Quere, Rep. Prog. Phys. **68**, 2495 (2005).
  - [2] T. Darmanin and F. Guittard, J. Mater. Chem. A **2**, 16319 (2014).
  - [3] L. Bocquet and J. L. Barrat, Soft Matter **3**, 685 (2007).
  - [4] J. P. Rothstein, Annu. Rev. Fluid Mech. **42**, 89 (2010).
  - [5] O. I. Vinogradova and A. L. Dubov, Mendelev Comm. **19**, 229 (2012).
  - [6] H. A. Stone, A. D. Stroock, and A. Ajdari, Annu. Rev. Fluid Mech. **36**, 381 (2004).
  - [7] M. Z. Bazant and O. I. Vinogradova, J. Fluid Mech. **613**, 125 (2008).
  - [8] F. Feuillebois, M. Z. Bazant, and O. I. Vinogradova, Phys. Rev. Lett. **102**, 026001 (2009).
  - [9] S. Schmieschek, A. V. Belyaev, J. Harting, and O. I. Vinogradova, Phys. Rev. E **85**, 016324 (2012).
  - [10] F. Feuillebois, M. Z. Bazant, and O. I. Vinogradova, Phys. Rev. E **82**, 055301(R) (2010).
  - [11] O. I. Vinogradova and A. V. Belyaev, J. Phys.: Cond. Matter **23**, 184104 (2011).
  - [12] D. Pimponi, M. Chinappi, P. Gualtieri, and C. M. Casciola, Microfluidics Nanofluidics **16**, 571 (2014).
  - [13] J. Ou, G. R. Moss, and J. P. Rothstein, Phys. Rev. E **76**, 016304 (2007).
  - [14] K. Kamrin, M. Bazant, and H. A. Stone, J. Fluid Mech. **658**, 409 (2010).
  - [15] A. V. Belyaev and O. I. Vinogradova, J. Fluid Mech. **652**, 489 (2010).
  - [16] J. Zhou, E. S. Asmolov, F. Schmid, and O. I. Vinogradova, J. Chem. Phys. **139**, 174708 (2013).
  - [17] N. V. Priezjev, J. Chem. Phys. **135**, 204704 (2011).
  - [18] C. Ybert, C. Barentin, C. Cottin-Bizonne, P. Joseph, and L. Bocquet, Phys. Fluids **19**, 123601 (2007).
  - [19] C. O. Ng, H. C. W. Chu, and C. Y. Wang, Phys. Fluids **22**, 102002 (2010).
  - [20] J. Zhou, A. V. Belyaev, F. Schmid, and O. I. Vinogradova, J. Chem. Phys. **136**, 194706 (2012).
  - [21] T. V. Nizkaya, E. S. Asmolov, and O. I. Vinogradova, Soft Matter **9**, 11671 (2013).
  - [22] N. V. Priezjev, A. A. Darhuber, and S. M. Troian, Phys. Rev. E **71**, 041608 (2005).
  - [23] E. Karatay, A. S. Haase, C. W. Visser, C. Sun, D. Lohse, P. A. Tsai, and R. G. H. Lammertink, PNAS **110**, 8422 (2013).
  - [24] O. I. Vinogradova, Int. J. Miner. Proc. **56**, 31 (1999).
  - [25] O. I. Vinogradova, K. Koynov, A. Best, and F. Feuillebois, Phys. Rev. Lett. **102**, 118302 (2009).
  - [26] L. Joly, C. Ybert, and L. Bocquet, Phys. Rev. Lett. **96**, 046101 (2006).
  - [27] D. Seo and W. A. Ducker, Phys. Rev. Lett. **111**, 174502 (2013).
  - [28] J. R. Philip, J. Appl. Math. Phys. **23**, 353 (1972).
  - [29] E. Lauga and H. A. Stone, J. Fluid Mech. **489**, 55 (2003).
  - [30] O. I. Vinogradova, Langmuir **11**, 2213 (1995).
  - [31] P. J. Hoogerbrugge and J. M. V. A. Koelman, Europhys. Lett. **19**, 155 (1992).
  - [32] P. Español and P. Warren, Europhys. Lett. **30**, 191 (1995).
  - [33] T. Soddemann, B. Dünweg, and K. Kremer, Phys. Rev. E **68**, 046702 (2003).
  - [34] J. Smiatek, M. Allen, and F. Schmid, Eur. Phys. J. E **26**, 115 (2008).
  - [35] E. S. Asmolov, J. Zhou, F. Schmid, and O. I. Vinogradova, Phys. Rev. E **88**, 023004 (2013).
  - [36] H. Limbach, A. Arnold, B. Mann, and C. Holm, Comput. Phys. Commun. **174**, 704 (2006).
  - [37] A. D. Stroock, S. K. Dertinger, G. M. Whitesides, and A. Ajdari, Anal. Chem. **74**, 5306 (2002).
  - [38] S. Wiggins and J. M. Ottino, Phil. Trans. R. Soc. A **362**, 1818, 937 (2004).
  - [39] H. Aref, Journal of Fluid Mechanics **143**, 1 (1984).
  - [40] M. A. Stremler, F. R. Haselton, and H. Aref, Phil. Trans. R. Soc. Lond. A **362**, 1019 (2004).